
Article:
Mullis, AM (2015) Spontaneous deterministic side-branching behavior in phase-field simulations of equiaxed dendritic growth. Journal of Applied Physics, 117 (11). 114305. ISSN: 0021-8979

https://doi.org/10.1063/1.4915278

Spontaneous deterministic side-branching behavior in phase-field simulations of equiaxed dendritic growth

Andrew M Mullis
Institute for Materials Research, University of Leeds, Leeds LS2-9JT, UK.

The accepted view on dendritic side-branching is that side-branches grow as the result of selective amplification of thermal noise and that in the absence of such noise dendrites would grow without the development of side-arms. However, recently there has been renewed speculation about dendrites displaying deterministic side-branching [see e.g. ME Glicksman, Metall. Mater. Trans A 43 (2012) 391]. Generally, numerical models of dendritic growth, such as phase-field simulation, have tended to display behaviour which is commensurate with the former view, in that simulated dendrites do not develop side-branches unless noise is introduced into the simulation. However, here we present simulations that show that under certain conditions deterministic side-branching may occur. We use a model formulated in the thin interface limit and a range of advanced numerical techniques to minimise the numerical noise introduced into the solution, including a multigrid solver. Spontaneous side-branching seems to be favoured by high undercoolings and by intermediate values of the capillary anisotropy, with the most branched structures being obtained for an anisotropy strength of 0.03. From an analysis of the tangential thermal gradients on the solid-liquid interface, the mechanism for side-branching appears to have some similarities with the deterministic model proposed by Glicksman.

1. Introduction

One of the most fundamental and all pervasive microstructures produced during the solidification of metals is the dendrite. The dendrite is a prime example of a pattern forming system where complex morphologies arise from initially homogeneous conditions due to the highly non-linear response of the controlling system. The formation of the secondary (and higher order) side-branches has been an area of particular interest as it is these secondary arms that give dendrites their characteristic morphology.

Imaging of dendritic growth in transparent analogue casting systems, such as succinonitrile [1] and xenon [2], show that close to the tip region the dendrite is apparently free from side-branching. Moving away from the tip small oscillations are initiated which grow as they move down the dendrite trunk. Initially the spacing of these perturbations is uniform. However, as amplification of the initial perturbations proceeds the process becomes competitive with faster growing side-arms becoming dominant, leading to a less uniform spacing. Eventually coarsening becomes dominant, with side-arms of higher curvature being preferentially re-melted [3, 4].

A number of measures have been proposed to quantify the side-branch morphology of dendritic structures. The simplest, and often the only measure that can be applied to as-solidified materials, is the secondary arm spacing, λ_2. However, when the growing dendrite can be imaged *in situ* a far greater range of measures may be applied. The most direct is $\bar{z}_{sb}$, which is the mean distance along the trunk (in units of ρ) at which the amplitude of the side-branching becomes equal to ρ, ρ being the radius of curvature at the dendrite tip. Other

measures which have been used in the literature [2, 5] to characterise dendritic structures include the fractal dimension, shape parameterization of the inner and outer side-branch envelopes, projection area and contour length.

Probably the most carefully controlled study of dendritic growth to be undertaken is the Isothermal Dendrite Growth Experiment [6] (IDGE), in which the onset of side-branching, as measured by the distance to the first detectable side-branch, was determined for high purity succinonitrile under microgravity conditions. This was determined as being at $(11.8 \pm 1.7)\rho$. In a control experiment, which was identical except that it was performed under terrestrial gravity, the same measurement yielded $(12.7 \pm 2.3)\rho$. Bisang & Bilgram [2] have measured $\bar{z}_{sb}$ for xenon dendrites under terrestrial conditions, finding $\bar{z}_{sb} = (17.5 \pm 3)\rho$. This figure is somewhat higher than that found during IDGE due to the different methodologies applied, the first detectable side-branch having an amplitude significantly less than 1ρ, wherein the two data sets are probably mutually consistent.

The generally accepted theory of side-branch formation during dendritic growth is that side-branches grow due to the selective amplification of thermally induced noise at the solid-liquid interface. Models for this process, in the framework of microscopic solvability theory, have been put forward by Langer [7, 8] and by Brener & Tempkin [9]. Such models appear to be supported by a number of phase-field simulations, in which it has been observed that dendrites grow without side-branches unless noise is introduced at the solid-liquid interface [10]. Where noise is introduced it is observed that the extent of side-branching (measured for instance by $\bar{z}_{sb}$) increases with both the amplitude of the noise and with the undercooling (or equivalently, velocity) at which the dendrite grows [11, 12], but decreases as the capillary anisotropy is increased.

However, models of deterministic side-branching have been proposed, such as that by [13], in which the dendrite experience repeated period doubling of an initially high frequency side-branching instability at the tip. Recently, based upon a re-evaluation of the IDGE data, Glicksman [14, 15] has proposed that dendrites may undergo deterministic side-branching. The proposition is that capillary mediated differences in the temperature along the solid-liquid interface give rise to heat currents (termed bias-fields) which lead to the onset of side-branching, even in the absence of thermally induced noise. It has been pointed out [16] that if an anisotropic capillary mediated temperature distribution is calculated for an exactly elliptic dendrite (although the same holds true for an exactly *parabolic* dendrite), a temperature inversion will arise near the tip for anisotropies exceeding 0.011, that is the lowest temperature is attained not at the tip, as would be the case for an isotropic surface energy, but at some point downstream of the tip. Moreover, even if the interface temperature decreases monotonically moving back from the dendrite tip, due to the curvature of the interface, the tangential thermal gradient is not unidirectional. It is proposed that where the bias-field exhibits a root, i.e. where the direction of the thermal gradient reverses, an inflection to the interface shape occurs. At this point there is an inward heat flow from both the dendrite tip and the downstream region. It is at this point at which deterministic side-branching is initiated. A geometrical analysis [17] shows these bias fields to be 4^{th}-order phenomenon in the interface shape, which may help explain the paucity of experimental evidence in support of the phenomena. As such they may be analogous to the surface species diffusion described by Mullins to explain the kinetics of thermal grooving at a grain boundary [18].

Contrary to most phase-field studies, Wang et al. [19] did find evidence of side-branching in the absence of artificially introduced noise for dendrites grown at the high undercooling of θ_{sys} = 0.8, apparently in support of the ideas proposed by [14, 15]. Here θ_{sys} is the dimensionless bulk undercooling, $\theta_{sys} = C_p\Delta T/H$, H being the latent heat on fusion and C_p the specific heat and would define the temperature boundary condition $\theta = -\theta_{sys.}$ However, such investigations are potentially fraught with pit-falls. In particular, unless considerable care is taken it is difficult to ensure that numerical noise is not introduced into the solution via the computational scheme employed. This is particularly the case when explicit solution schemes of the forward Euler type are used. Moreover, if a fixed (stability limited) time-step is utilised, the amplitude of the introduced noise increases at high undercooling due to lose of accuracy as the dendrite grows further per time-step.

In this paper we re-evaluate the findings of [19], using a thermal phase-field model formulated using a range of advanced numerical techniques designed to minimise the noise introduced in to the solution by the numerical scheme. In particular, we use an implicit time-stepping scheme with a non-linear multigrid solver which is a particularly efficient way of obtaining low noise solutions to a set of coupled partial differential equations. Typically, a Jacobi or Gauss-Seidel iteration is efficient at smoothing noise at wavelengths comparable to the mesh spacing, h, but very inefficient at smoothing noise at longer wavelengths, which therefore tends to remain in the solution. In multigrid, the restriction of the solution to progressively coarser nested meshes means that noise at all wavelengths is efficiently smoothed. Moreover, the time-step in the implicit solution is limited by the accuracy of the solution, not its stability. Therefore, by employing a dynamically adjusting variable time-step determined by a series of error estimators based upon the norm of the residuals in the solution we can ensure that the same level of accuracy is obtained in all solutions irrespective of the growth rate.

2. Computational Model

The model adopted here is based upon that of [20] in which, following non-dimensionalization against characteristic length and time scales, W_0 and τ_0, the evolution of the phase-field, ϕ, and the dimensionless temperature field, θ, are given by

$$A^2(\psi)\frac{\partial\phi}{\partial t} = \nabla\cdot\left(A^2(\psi)\nabla\phi\right) + \phi(1-\phi^2) - \lambda\theta(1-\phi^2)^2 - \frac{\partial}{\partial x}\left(A(\psi)A'(\psi)\frac{\partial\phi}{\partial y}\right) + \frac{\partial}{\partial y}\left(A(\psi)A'(\psi)\frac{\partial\phi}{\partial x}\right) \quad (1)$$

$$\frac{\partial\theta}{\partial t} = \alpha\nabla^2\theta + \frac{1}{2}\frac{\partial\phi}{\partial t} \quad (2)$$

where ψ is the angle between the principal growth direction and the outward pointing normal to the solid-liquid interface (the $\phi = 0$ isoline), d_0 is the chemical capillary length, k_E is the equilibrium partition coefficient, α is the dimensionless thermal diffusivity and λ is a coupling parameter given by $\lambda = \alpha/a_2 = a_1 W_0/d_0$ with a_1 and a_2 taking the values $5\sqrt{2}/8$ and 0.6267 respectively [21].For 4-fold growth, $A(\psi) = 1 + \varepsilon.\cos(4\psi)$, where ε is a measure of the anisotropy strength.

The governing equations are discretized using a finite difference approximation based upon a quadrilateral, non-uniform, locally-refined mesh with equal grid spacing in both directions. Unlike the implementation of most phase-field models, which use spatially second order difference approximations, here we have used fourth order approximations in order to capture any bias-field effects, which are themselves proposed to be spatially fourth order [17]. The first and second differentials are calculated using a (spatially) fourth order accurate 9-point stencil, while a compact, 17-point, fourth order stencil has been used for the Laplacian terms, compact stencils being superior in their ability to reduce the mesh induced [22] anisotropy. The stencils, and the weights associated with each point therein, are illustrated graphically in Fig. 1. To ensure sufficient mesh resolution around the interface region local mesh refinement (coarsening) is employed when the weighted sum of the gradients of ϕ and θ exceeds (falls below) some predefined value.

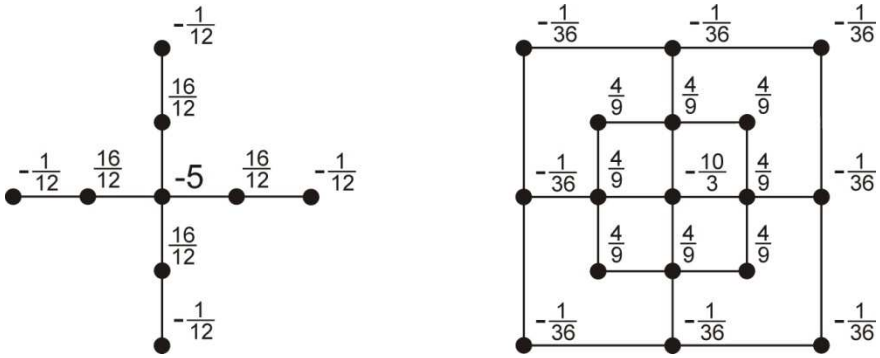

Figure 1. 9 and 17-point finite difference stencils used to evaluate the second differentials and Laplacian terms in Equations (1-2).

The most commonly employed temporal discretization schemes utilised in phase-field modelling are explicit methods such as the Forward Euler scheme, which is first order accurate in time. Rewriting Equations (1) and (2) in operator form

$$\frac{\partial \phi}{\partial t} = F_\phi(t,\phi,\theta), \quad \frac{\partial \theta}{\partial t} = F_\theta\left(t,\theta,\frac{\partial \phi}{\partial t}\right) \tag{3}$$

the forward Euler scheme can be written as

$$\begin{bmatrix} \phi^{k+1} \\ \theta^{k+1} \end{bmatrix} - \begin{bmatrix} \phi^{k} \\ \theta^{k} \end{bmatrix} = \Delta t \begin{bmatrix} F_\phi\left(t^k,\phi^k,\theta^k\right) \\ F_\theta\left(t^k,\theta^k,\dot{\phi}^{k+1}\right) \end{bmatrix} \tag{4}$$

The implementation of explicit methods is straight forward, but they suffer from a number of restrictions, including a time-step that is limited by stability, rather than accuracy, and a tendency to introduce numerical noise into the solution of the set of PDE's being considered. In contrast, implicit methods may be designed to be unconditionally stable, wherein the time-step may be chosen in order to achieve a desired level of accuracy in the solution. Here, we have used the second order Backward Difference Formula (BDF2), which is an implicit linear 2-step method which leads to second order convergence in time. It can be shown that the BDF2 method is A-stable [23], and is therefore suitable for stiff systems of differential equations. With a variable time step of ratio, $r = \Delta t_k/\Delta t_{k-1}$, the BDF2 equivalent of Equ. (4) is

$$\frac{1+2r}{1+r}\begin{bmatrix}\phi^{k+1}\\ \theta^{k+1}\end{bmatrix}-(r+1)\begin{bmatrix}\phi^{k}\\ \theta^{k}\end{bmatrix}+\frac{r^2}{1+r}\begin{bmatrix}\phi^{k-1}\\ \theta^{k-1}\end{bmatrix}=\Delta t\begin{bmatrix}F_\phi\left(t^{k+1},\phi^{k+1},\theta^{k+1}\right)\\ F_\theta\left(t^{k+1},\theta^{k+1},\dot{\phi}^{k+1}\right)\end{bmatrix} \tag{5}$$

The choice of appropriate time steps is based upon a set of local error estimators

$$D_k^\phi=\frac{r}{r+1}\left\|\phi^{k+1}-(1+r)\phi^k+r\phi^{k-1}\right\|_\infty \tag{6}$$

$$D_k^\theta=\frac{r}{r+1}\left\|\theta^{k+1}-(1+r)\theta^k+r\theta^{k-1}\right\|_\infty \tag{7}$$

Each of the error estimators is compared against a corresponding tolerance (D_{Tol}^ϕ, D_{Tol}^θ) and if at any time-step the local temporal error $D_k = \min(\ D_{Tol}^\phi\ ,\ D_{Tol}^\theta\ ) \le D_{Tol}$ the time step is accepted and the next time-step is increased whereas if $D_k \ge D_{Tol}$ the step is rejected and retaken with a smaller time-step. In this way the accuracy of the solution is maintained, even when the solidification rate increases, as for instance at high undercooling or during the initial transient when the seed used to nucleate solidification is coming into thermal equilibrium with the domain. The rate at which the time-step should grow can be estimated from

$$r=\left(\frac{D_{Tol}}{D_k}\right)^{\frac{1}{1+p}} \tag{8}$$

where p is the order of the scheme, which is 2 for the BDF2 method.

When using implicit time-stepping methods it is necessary to solve a very large, but sparse, system of non-linear algebraic equations at each time-step. Multigrid methods are among the fastest available solvers for such systems and in this work we apply the non-linear generalization known as FAS (full approximation scheme [24]). The local adaptivity is accommodated via the multilevel algorithm originally proposed by Brandt [25]. The interpolation operator is bilinear while injection is used for the restriction operator. For smoothing the error we use a fully-coupled nonlinear weighted Gauss-Seidel iteration where the number of pre- and post-smoothing operations required for optimal convergence is determined empirically. Full details of the numerical scheme are given in [26, 27].

The resultant dendrite shapes are characterised by two length scales, the actual and parabolic radii of curvature at the tip, ρ_a and ρ_{para} respectively. Here, if (X, Y) is the locus of the solid-liquid interface, ρ_a is given, for a dendrite growing along the x-direction, by

$$K=\frac{\partial^2 X/\partial Y^2}{\left(1+\left(\partial X/\partial Y\right)^2\right)^{3/2}}\ ,\qquad \rho_a=\frac{1}{|K|} \tag{9}$$

For a dendrite with tip location X_0, the parabolic tip radius is given by fitting a curve of the form

$$Y^2 = -2\rho_{\text{para}}(X - X_0) \tag{10}$$

to the down-stream region of the dendrite, typically the region $1.5\rho_a - 4.0\rho_a$ behind the tip (ρ_a is used in determining the range for the fitting as it can be known prior to determining ρ_{para}). The procedure for calculating ρ_{para} is given in more detail in [20].

3. Numerical Results

Figure 2 compares the morphology of the solid-liquid interface for dendrites grown at $\theta_{\text{sys}} = 0.6875$ and $\theta_{\text{sys}} = 0.8000$, the other computational parameters for these simulations being $\alpha = 1$, $\varepsilon = 0.03$ and $h = 1.24d_0$. The domain size, Ω, is $[-2500d_0{:}2500\ d_0]^2$ and the initial seed with radius $8d_0$ is located at the centre of the domain. It is apparent that from the plots that spontaneous side-branching is occurring at the higher undercooling but not at lower undercooling. While superficially these results look similar to those of [19] there are two important differences. Firstly, although [19] present images (e.g. their Figs. 2a and 3a) showing equiaxed dendrites with 4-fold symmetry, their simulations are in fact conducted on a quarter domain with the equiaxed dendrite being created by rotating and replicating a single primary branch. In contrast, the equiaxed dendrite shown in this work (Fig. 2b) is nucleated from a seed in the middle of the domain. Each of the primary arms shown has therefore grown independently and the fact that each shows an identical branching pattern in itself represents strong evidence of a deterministic branching mechanism as numerical noise, by its random nature, would give rise to different patterns on each primary branch. Secondly, in [19] very low anisotropies are used in order to obtain branching. In their work strong branching is evident at $\varepsilon = 0.005$, with branching becoming almost indiscernible at $\varepsilon = 0.02$. It is well known that noise induced side-branching is suppressed by strong capillary anisotropy. In contrast the branched dendrite shown in Fig. 2b is grown at the relatively high anisotropy of $\varepsilon = 0.03$. For reference the tip radii for the two simulations being considered here are $\rho_a = 13.6d_0$, $\rho_{\text{para}} = 25.0d_0$ for $\theta_{\text{sys}} = 0.6875$ and $\rho_a = 11.8d_0$, $\rho_{\text{para}} = 20.9d_0$ for $\theta_{\text{sys}} = 0.8000$.

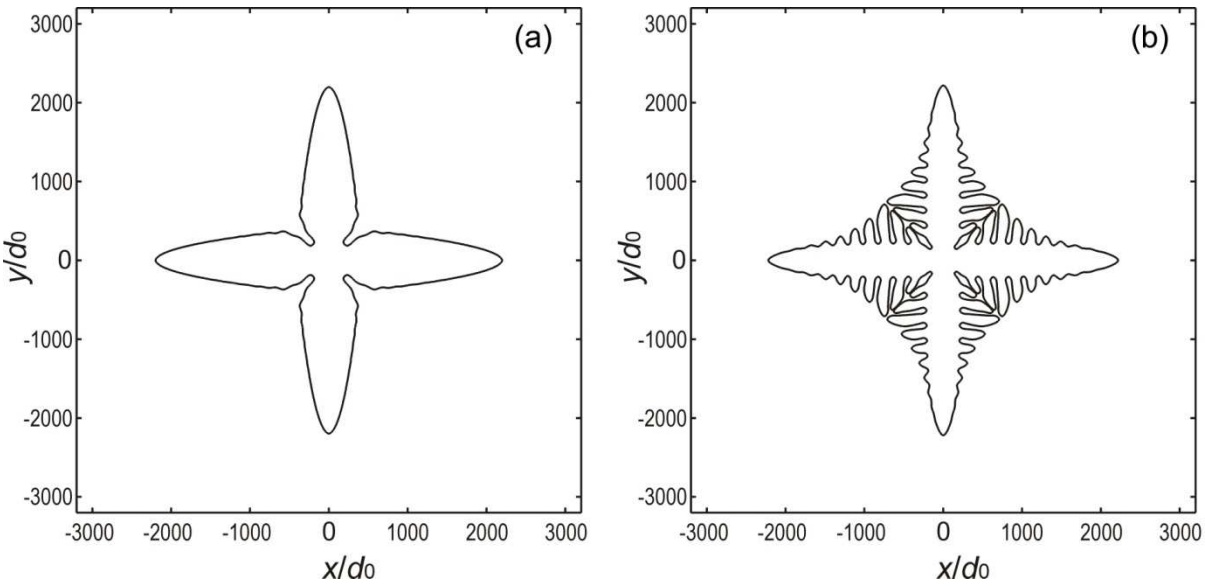

Figure 2. Example phase-field dendrite morphologies at a system undercooling of (a) $\theta_{\text{sys}} = 0.6875$, without side-branching and (b) $\theta_{\text{sys}} = 0.8000$, displaying spontaneous side branching.

The effect of anisotropy on the tendency towards spontaneous side-branching is explored in Fig. 3. We use two different measures for this, on the left-hand y-axis we plot the dimensionless undercooling, θ_{sys}, required for the onset of spontaneous side-branching, while on the right-hand y-axis is plotted the measured value of $\bar{z}_{sb}$ determined at a fixed undercooling of $\theta_{sys} = 0.8000$. Here, $\bar{z}_{sb}$ is defined with respect to the parabolic tip radius, ρ_{para}, as this is more readily comparable to the tip radius that can be measured in experiments on transparent analogue systems. The outcome is somewhat contradictory. We find that the minimum value of θ_{sys} required for the onset of spontaneous side-branching, which we denote by θ_{onset}, decreases monotonically with increasing ε, but that the most branched structures (as measured by $\bar{z}_{sb}$) occur at intermediate values of ε. Indeed, it is apparent from the plot of $\bar{z}_{sb}$ as a function of ε that the trend is approximated well by two linear trend lines, intersecting at $\varepsilon = 0.03$. This suggests that the mechanism responsible for the observed side-branching is not the same as operating in the simulations reported by [19] and is not related to the amplification of numerical noise, wherein side-branching would become more extensive (i.e. both the minimum value of θ_{sys} and the measured value of $\bar{z}_{sb}$ would decrease) as ε decreases. A potential explanation for this observation will be proposed towards the end of this manuscript.

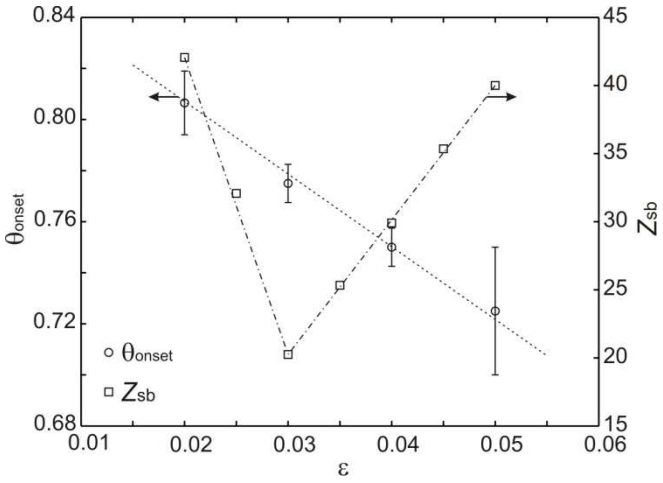

Figure 3. The undercooling, θ_{onset}, at which spontaneous side-branching is first observed, and the extent of side-branching, as measure by $\bar{z}_{sb}$, both plotted as a function of the imposed anisotropy, ε.

To investigate the mechanism for side-branch formation in these simulated dendrites and to explore the similarities with the deterministic side-branching mechanism proposed in [14, 15] it is instructive to look in some detail at the temperature distribution at the dendrite tip. Figure 4 compares (a) the temperature distribution obtained when an anisotropic surface energy is imposed upon an exactly parabolic needle crystal with (b) the temperature distribution obtained from a phase-field dendrite (b). In both cases $\varepsilon = 0.03$ and in the phase-field simulation $\theta_{sys} = 0.6875$. The temperature distribution for the parabolic needle was obtained by (i) generating an exact parabola; (ii) calculating its curvature and hence the temperature at its interface; (iii) bringing the shape into thermal equilibrium, treating the temperature calculated in (ii) above as a Dirichlet boundary condition on the solid-liquid interface. It can

be observed that in the case of the exactly parabolic needle there is indeed a temperature inversion, with the lowest temperature occurring either side of the tip. In contrast, for the phase-field dendrite no such temperature inversion is observed, with the tip being the region with the lowest temperature. In deed, in no phase-field simulation, irrespective of the undercooling at which the dendrite is grown or the anisotropy imposed upon the system, have we observed a temperature inversion on the solid-liquid interface, with the tip region always being the region lowest temperature.

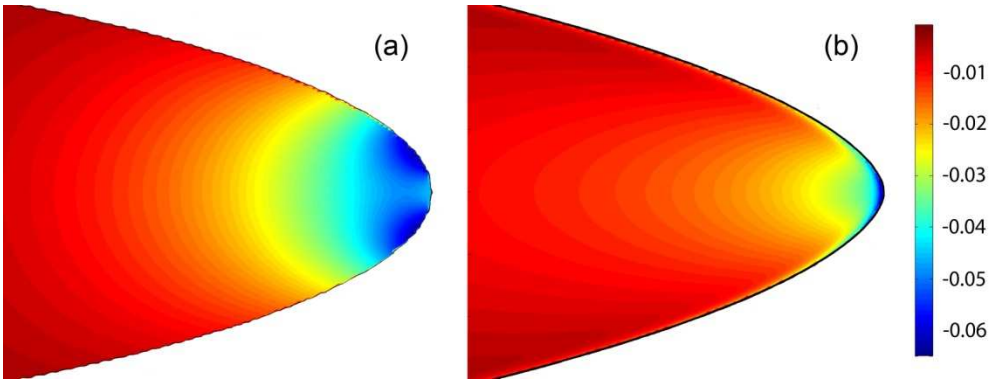

Figure 4. Thermal profile in the tip region of (a) an exactly parabolic dendrite with an anisotropic surface energy (ε = 0.03) and (b) a phase-field dendrite growing with a surface energy anisotropy of $\varepsilon = 0.03$.

The absence of a temperature inversion near the tip of the phase-field dendrite appears to be because the shape of the dendrite tip alters in response to the imposed anisotropy in such a way that such an inversion is avoided. Specifically, as the anisotropy is increased the curvature increases more rapidly as one approaches the tip than would be the case for an equivalent exactly parabolic crystal. This can be seen most readily by comparing the actual and parabolic radii of curvature, ρ_a and ρ_{para} respectively, for the phase-field dendrites. In Figure 5 we plot the ratio $\rho_{\text{para}}/\rho_a$ as a function of system undercooling and anisotropy. It can be seen that the ratio $\rho_{\text{para}}/\rho_a$ increases rapidly with increasing ε while there is a much smaller variation as a function of undercooling, i.e. that as the anisotropy increases the tip region sharpens more rapidly than would be expected from the near parabolic down-stream shape, thus avoiding a temperature inversion at the tip.

However, as pointed out in [14, 15], due to the curvature of the solid-liquid interface the tangential thermal gradient evaluated on the interface may not be monotonic, even if the temperature does decrease monotonically moving down-stream from the tip. For the phase-field model, in which the temperature and phase fields are defined over the whole domain, this tangential surface thermal gradient may be evaluated using standard methods for directional derivatives, wherein $\hat{\Phi}$ may also be defined over the whole domain by,

$$\hat{\Phi} = \frac{\phi_x \theta_y - \phi_y \theta_x}{|\nabla \phi|^2} \tag{11}$$

However, we will consider only the values occurring on the $\phi = 0$ isoline, wherein the definition is equivalent to that used in [14, 15]. Here the subscripts denote differentiation with respect to x or y respectively. A plot of $\hat{\Phi}$, non-dimensionalised against d_0, as a function of the distance downstream from the dendrite tip is shown in Fig. 6, for the dendrite not displaying side-branching in Fig. 2a. The similarity in the form of the curve shown in Fig. 6, calculated for a phase-field dendrite, with the profiles calculated analytically by Glicksman [see e.g. Fig. 5 in Ref. 14] is remarkable. In particular, in both cases the curve has a turning point somewhat downstream from the tip and it is this turning point in the tangential thermal gradient which [14, 15] has associated with the deterministic side-branching mechanism. Note that the co-ordinate system used here is different from that in [14, 15] in which an elliptic geometry was considered.

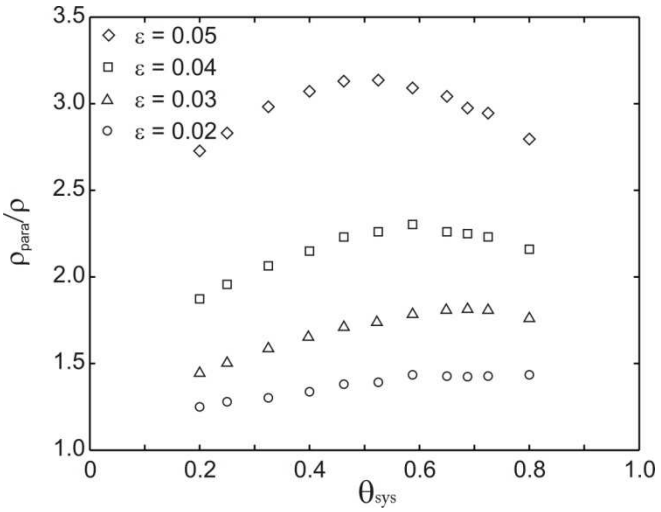

Figure 5. Ratio of the parabolic to the actual tip radius as a function of undercooling and anisotropy. The increase in the ratio, ρ_{para}/ρ_a, with increasing anisotropy appear to be a consequence of the tip becomes progressively sharper, relative to the down-stream parabolic profile.

In this particular case we have shown as an example the tangential thermal gradient, $\hat{\Phi}$, corresponding to a dendrite that does not display spontaneous side-branching, although the form of the curve in the near-tip region is similar, irrespective of whether side-branching is well developed down-stream or not. The principal difference in the curves as either the undercooling, θ_{sys}, or the anisotropy, ε, is increased is that the minimum become deeper. This is illustrated in Fig. 7 in which we give the magnitude, $\left|\hat{\Phi}\right|$, of the minimum in the tangential thermal gradient as a function of θ_{sys} and ε. In absolute co-ordinates, (i.e. in units of d_0), the location of the minimum moves closer to the tip as either θ_{sys} or ε is increased, although this appears to be related to a reduction in the characteristic length scale of the dendrite, as measured by either ρ_a or ρ_{para}. In particular, when the distance is scaled against ρ_a, which close to the tip is probably the most appropriate length scale, the minimum tends to occurs in the range $0.10\rho_a - 0.15\rho_a$, hence the use of ρ_a as the length scale on the x-axis in Fig. 7. Although there is some scatter within the range $0.10\rho_a - 0.15\rho_a$, there does not appear to be a systematic trends with either undercooling nor anisotropy, and we believe the scatter may be

due to the extent to which the tip is resolved on the mesh and the interpolation of the location of the $\phi = 0$ isoline.

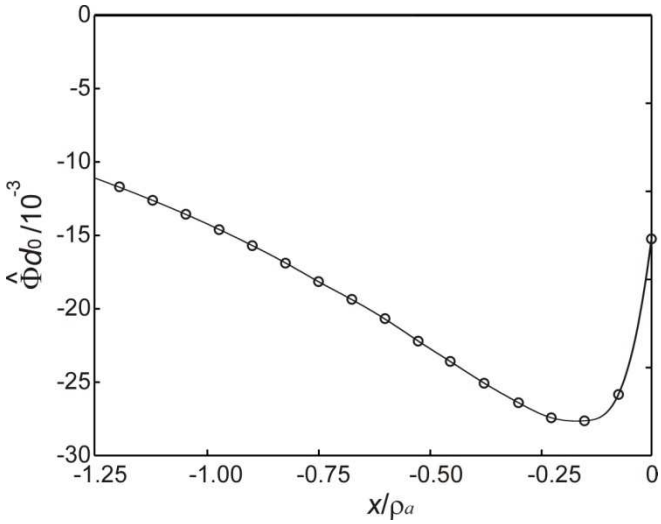

Figure 6. The tangential thermal gradient calculated on the solid-liquid interface near the tip-region for a dendrite with $\theta_{sys} = 0.6875$ (Fig. 2a above).

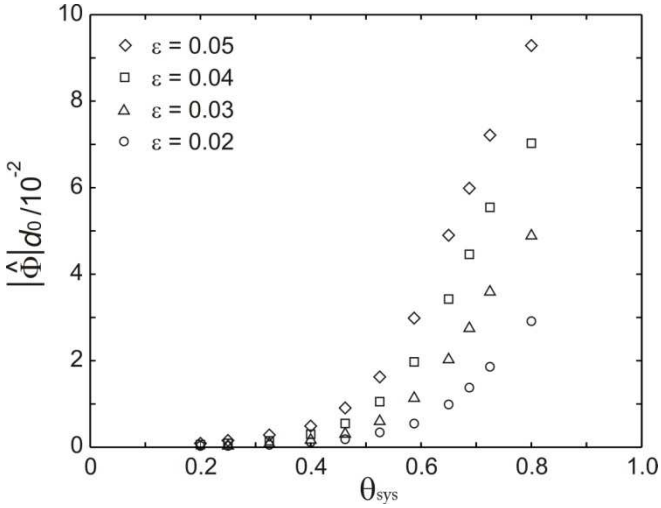

Figure 7. The magnitude of the minimum in the tangential thermal gradient, calculated on the solid-liquid interface near the tip-region, as a function of undercooling, θ_{sys}, and anisotropy, ε.

Given that the tangential thermal gradient on the interface has a similar form for all of the phase-field dendrites calculated, but that only those growing at high undercooling go on to develop spontaneous side-branches, it is interesting to consider whether the tangential thermal gradient leads to any perturbation of the dendrite shape close to the tip, as proposed in [14, 15]. This will help elucidate whether these effects are thereby having an effect leading to observable side-branching further downstream. To determine this the following procedure has been adopted. The tip region of the dendrite (from $X - X_0 = 0$ to $X - X_0 \approx -160 d_0$) has been fitted with an order n polynomial, where n is 4-5. This is of sufficiently high order to capture

the non-parabolic tip shape but not of sufficiently high order to capture perturbations to the tip-shape from side-branching. We have then calculated the residuals between the fit and the original data to identify small perturbations to the dendrite shape. The results of this analysis for θ_{sys} = 0.6875 (a dendrite not showing spontaneous side-branching) are shown in Fig. 8, wherein it can be seen that there is indeed a cyclic perturbation to the dendrite tip shape. Similar perturbations are also found where the dendrite does show distinct downstream side-branching, although unlike the case shown in Figure 8, the amplitude of the perturbations tends to increase, rather than decrease, with distance downstream. As with the tangential thermal gradient, the form of this curve is similar irrespective of either the undercooling or anisotropy at which the dendrite is growing, although the magnitude of the shape perturbations, as measured by the residual, appears to increase as the magnitude of the tangential gradient increases (i.e. with increasing undercooling or anisotropy).

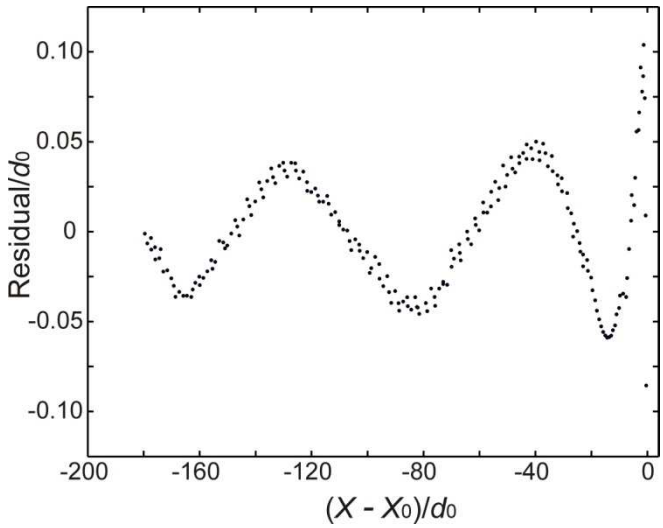

Figure 8. Residual between the actual shape of a phase-field dendrite grown at θ_{sys} = 0.6875 and an order 4 polynomial fit to the tip region. This procedure is very efficient at showing up small cyclic perturbations to the tip region.

We also note that the period of the final, well developed side-branches is almost exactly double the period of the initial perturbation in all cases. In this respect there are interesting parallels with the model of [13], in which a period doubling of the initial side-branching instability was also identified. Moreover, for anisotropies of $\varepsilon \leq 0.030$ (to the left of the minimum in Fig. 3) there is no vestige of the eliminated perturbations in the final microstructure. However, for $\varepsilon > 0.035$ (to the right of the minimum in Fig. 3) we notice that small vestiges of the initial perturbation remain, in the form of poorly developed side-branches which are located in between the main, well-developed branches. An example of this type of morphology is shown in Fig. 9 for a dendrite grown with an anisotropy of $\varepsilon = 0.045$ and at an undercooling of θ_{sys} = 0.8. The subsidiary side-branches are indicated with arrows for clarity. Although it is well established that secondary arm coarsening proceeds by the dissolution of unfavourable branches from the tip back towards the trunk [28, 29], this appears not to be the case here, as the branches never fully develop. Instead, these appear to be remnants indicative of a period doubling instability as described by [13].

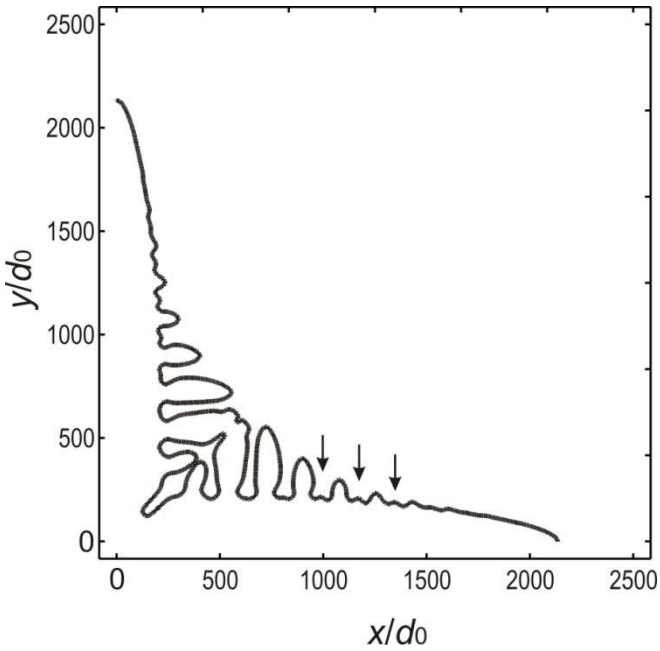

Figure 9. Spontaneous side branching pattern for a dendrite with $\varepsilon = 0.045$ and θ_{sys} = 0.8. The spacing of the well developed side-branches in twice the wavelength of the perturbations at the tip with small vestiges of side-branches (indicates with arrows) the only indication of the shorter wavelength of the initial perturbation.

4. Discussion

The overall picture that emerges seems to be as follows;

1) Using a spatially 4th-order accurate phase-field model it can be shown that under certain circumstance some, but by no means all, simulated dendrites will display spontaneous, deterministic side-branching.
2) Due to the inclusion of a low-noise multigrid solver we can have reasonable confidence that this side branching is not due to the amplification of numerical noise.
3) The occurrence of spontaneous side branching is restricted to high undercooling.
4) The affect of increasing the anisotropy is quite subtle. If we measure the undercooling at which spontaneous side-branching can be first observed we would conclude that high anisotropy favours spontaneous side-branching. Conversely, if we measure the extent of side-branching at fixed undercooling (for instance by $\bar{z}_{sb}$), we would conclude that intermediate anisotropy favours spontaneous side-branching. Neither result is compatible with the amplification of numerical noise.
5) If we calculate a low order polynomial fit (n = 4 – 5) to the dendrite tip region, cyclic perturbations to the dendrite shape appear to occur all the way up to the tip. This appears to be true irrespective of whether the dendrite goes on to develop visible side-branching or not.
6) If we calculate the tangential thermal gradient along the solid-liquid interface ($\phi = 0$ isoline) of the dendrite in the near-tip region we find that such gradients have a form very similar to those calculated analytically by Glicksman [14, 15], which he has

postulated gives rise to deterministic side-branching during the growth of anisotropy free elliptic dendrite fragments.

We believe the above observations may be reconciled in the following manner. Where we have previously introduced noise into phase-field simulations to generate side-branching [11] we observe that a critical amplitude exists and that the noise introduced must have an amplitude exceeding this critical value if observable side-branched are to develop. The value of this critical amplitude increases with increasing anisotropy. We postulate that the bias-fields introduced by Glicksman are a perturber of the interface shape, that is they act as a source of deterministic 'noise' on the solid-liquid interface. The amplitude of this noise, i.e. the magnitude of $\hat{\Phi}$, increases with increasing undercooling, hence the tendency for deterministic side-branching to be more readily observed at high undercooling. As the anisotropy is increased the amplitude of the noise also increases, but so does the ability of the dendrite to resist side-branching. This could be either due to the a threshold value that the noise must exceed increasing with increasing anisotropy or due to the rate of amplification of small interface perturbations decreasing with increasing anisotropy. What we are seeing in Fig. 3 with regard to $\bar{z}_{sb}$ would thus be a result of a competition between a noise whose amplitude were increasing with anisotropy and an amplification threshold (rate) that were increasing (decreasing) with increasing anisotropy. This may also be responsible for the difference between the morphology of branched dendrites with $\varepsilon > 0.035$, in which small vestiges of intermediate side-branches are present reflecting the doubling of the initial period of the tip perturbation and those with $\varepsilon \leq 0.030$, in which this period doubling occurs without leaving remnant side-branches.

The model proposed here therefore has a common underlying principle to the bias-field model proposed by Glicksman, but also some key differences. In particular, Glicksman postulates that deterministic side-branching may occur at all undercoolings, which is not consistent with the results presented here where such side-branching is restricted to high undercoolings. We believe that the origin of this discrepancy is that in the calculations presented by Glicksman, anisotropy is either absent, or is not included in a consistent manner. By this we mean that even when a temperature distribution corresponding to an anisotropic surface energy is considered, it is then imposed upon a simple model dendritic shape, rather than the free boundary shape calculated from the specified surface energy. We can see from Fig. 5 and from the argument above, that increasing the anisotropy strength has two competing effects, these being to increase the size of the shape perturbation at the dendrite tip and to increase the resistance of the dendrite to amplification of these perturbations. In the (unphysical) limit of vanishing anisotropy it is open to question which effect dominates. Conversely, increasing the undercooling increase the size of the shape perturbation at the dendrite tip and may also reduce the effective anisotropy. Consequently, if the ability of the dendrite to resist the amplification of small perturbation into full side-branches vanishes with vanishing anisotropy but the size of the perturbations at the tip does not, it would be expected that an isotropic calculation would conclude that side branching could be observed at all undercoolings.

5. Summary and Conclusions

By using a phase-field model incorporating a range of advanced numerical techniques designed to achieve high solution accuracy with minimal induced numerical noise we have been able to demonstrate that under certain circumstances dendrites may undergo spontaneous, deterministic side-branching. Calculation of the tangential thermal gradients on the phase-field solid-liquid interface appears to be consistent with the capillary mediated 'bias-field' branching mechanism proposed by Glicksman [14, 15]. The occurrence of such side-branching appears to be confined to relatively high undercooling/growth velocity. We suggest that this mechanism probably acts alongside the more conventionally accepted thermal noise mechanism for generating the initial perturbations that give rise to dendritic side-branching. If so, this could potentially suggest an interesting area of investigation in experimental solidification, exploring whether it is possible to observe a transition from stochastic to deterministic side-branching in deeply undercooled metallic melts or analogue casting systems.

6. References

[1] D. P. Corrigan, M. B. Koss, J. C. La Combe, K. D. DeJager, L. A. Tennenhouse and M. E. Glicksman, *Phys. Rev. E* **60** 7217 (1999).
[2] U. Bisang and J. H. Bilgram, *Phys. Rev. E* **54** 5309 (1996).
[3] T. Z. Kattamis, J. C. Coughin and M. C. Flemings, *Trans. Met. Soc. AIME* **239** 1504 (1967).
[4] K. P. Young and D. H. Kirkwood, *Met. Trans.* **6A** 197 (1975).
[5] Q. Li and C. Beckermann, *Phys. Rev. E* **57** 3176 (1998).
[6] L. A. Tennerhouse, M. B. Koss, J. C. LaCombe and M. E. Glicksman, *J. Cryst. Growth* **174** 82 (1997).
[7] M. N. Barber, A. Barbieri and J. S. Langer, *Phys Rev. A* **36** 3340 (1987).
[8] J. S. Langer, *Phys. Rev. A* **36** 3350 (1987).
[9] E. Brener and D. Temkin, *Phys. Rev. E* **51** 351 (1995).
[10] J. A. Warren and W. J. Boettinger, *Acta metall. mater.* **43** 689 (1995).
[11] A. M. Mullis, *Acta mater.* **49** 2205 (2001).
[12] A. M. Mullis, *Acta mater.* **51** 1959 (2003).
[13] P.K. Galenko, D.M. Krivilyov and S.V. Buzilov, *Phys. Rev. E* **55** 611 (1997).
[14] M. E. Glicksman, 'Coherent Capillary-mediated dendritic branching', in *Proc. MCWASP XIII (Schladming, Austria, 17–22 June 2012) IOP Conf. Series: Materials Science and Engineering* **33** 012097 (2012).
[15] M. E. Glicksman, *Metall. Mater. Trans*. **43A** 391 (2012).
[16] M. E. Glicksman, Oral presentation at *MCWASP XIII (Schladming, Austria, 17–22 June 2012)*.
[17] M. E. Glicksman, 'Capillary bias-fields and interface branching' *TMS 2014 - 143rd Annual Meeting & Exhibition: Supplemental Proceedings (16–20 Feb. 2014, San Diego, CA)* pp 753-767, TMS-Wiley, Hoboken, NJ, ISBN: 978-1-118-88972-5 (2014).
[18] W. W. Mullins, *J. Appl. Phys.* **28** 333 (1957).
[19] Z. Wang, J. Wang and G. Yang, *Phys. Rev. E* **78** 042601 (2008).
[20] J. Rosam, P. K. Jimack and A. M. Mullis, *Acta Mater*. **56** 4559 (2008).
[21] A. Karma , *Phys. Rev. Lett*. **87** 115701 (2001).
[22] A. M. Mullis, *Comp. Mater. Sci.* **36** 345 (2006).
[23] W. Hundsorfer & J.G. Verwer, Numerical Solution of Time-Dependant Advection-Diffusion-Reaction Equations, Springer-Verlag, (2003).

[24] U. Trottenberg, C. Oosterlee and A. Schuller, *Multigrid* (Academic Press, London, 2001).
[25] A. Brandt, *Math. Comp*. **31** 333 (1977).
[26] J. Rosam, P. K. Jimack and A. M. Mullis, *J. Comp. Phys*. **225** 1271 (2007).
[27] A. M. Mullis, *Phys. Rev. E* **79** 030601 (2009).
[28] D. H. Kirkwood, *Mater. Sci. Eng*. **73** L1 (1985).
[29] A.M. Mullis, *Acta Mater*. **46** 4609 (1998).